Available online at www.sciencedirect.com
SCIENCE DIRECT®
International Journal of Heat and Mass Transfer 48 (2005) 1747–1759
International Journal of HEAT and MASS TRANSFER
www.elsevier.com/locate/ijhmt

The thermal efficiency of near-wall gas-droplets screens. Part I. Numerical modeling

V.I. Terekhov *, M.A. Pakhomov [1]

Kutateladze Institute of Thermophysics Sib. Branch Russian Academy of Sciences, 1, Acad. Lavrentyev Avenue, 630090 Novosibirsk, Russia

Received 16 November 2004
Available online 26 January 2005

Abstract

Present work is directed to further perfection of a modeling of the structure and heat transfer processes in gas-droplets near-wall screens in a tube. The problem statement in the present work is based on the Eulerian–Eulerian two-fluid model for transport processes in the gas and dispersed phases in the turbulent gas-droplets jet. We used the model [High Temp. 40(1) 2002 78] for computation of averaged motion, heat transfer and squared velocity fluctuations of dispersed phase. The gas phase turbulence was modeled with the LRN k–$\widetilde{\varepsilon}$ [AIAA J. 36(1) 1998 38] model with taking into account the effect of evaporating droplets on the kinetic turbulence energy and the rate of its dissipation. The present paper takes into account the influence of droplets deposition and vaporization of deposited particles on the tube wall and particles evaporation in the near-wall jet. Developed numerical model was tested by comparison with experimental and numerical data for gas-droplets non-isothermal flow in a tube and in a near-wall screen.

1. Introduction

The thermal shielding of walls from the destructive action of high-enthalpy or reactive flows with the help of wall screens is an urgent problem of importance in developing various apparatuses and facilities. In many practical cases, highly efficient are hydrodynamic methods for thermal protection of channel walls, which use injection of a protecting gas (liquid) into the boundary layer through the wall surface. The simplest approach here is injection of a protecting gas (liquid) through a tangential slot. In this case, either a co-current an oppositely directed secondary flow can be organized. Since, nowadays, the temperature of working media in combustion chambers and other calorifically intense components of various apparatus permanently increases, thermal protection of wall surfaces still remains a very important matter.

The theory of single-phase screens both in relatively simple and more complex dynamic conditions is a well-developed theory whose foundations were outlined in [1–5]. The main approaches used in developing the theory of single-phase screens are worth noting. Those are works based on using the integral relations for turbulent boundary layer [1–4,6] or the Prandtl

* Corresponding author. Tel.: +7 3832 341736/328969; fax: +7 3832 343480.
E-mail addresses: terekhov@itp.nsc.ru (V.I. Terekhov), pakhomov@ngs.ru (M.A. Pakhomov).
[1] Tel.: +7 3832 391336/244079; fax: +7 3832 343480.

0017-9310/$ - see front matter © 2005 Elsevier Ltd. All rights reserved.
doi:10.1016/j.ijheatmasstransfer.2004.11.010

Nomenclature

$A = \frac{(x-x_0)}{Sm} Re_S^{0.25}$ parameter

$b_{1D} = (K_{VS} - K_V)/(1 - K_{VS})$ diffusional injection parameter for the vapor released by an evaporation, which should be found from the saturation curve

C_D coefficient of resistance

C_p, C_{pA}, C_{pL}, C_{pV} heat capacities of mixture, air, liquid, and vapor (J/kg K)

D vapor diffusivity in air (m^2/s)

D_{xL}, D_{rL} turbulent diffusivities of drops in the axial and radial directions due to the stochastic motion of drops and their entrainment into the gas flow by intense vortices (m^2/s)

d droplet diameter (m)

d_P particle diameter (m)

g gravitational acceleration (m/s^2)

g_k, g_ε coefficients of droplet entrainment into the micropulsational motion of the gas flow

H enthalpy (J/kg)

J mass flux of vapor from the surface of evaporating droplet ($kg/m^2 s$)

k turbulent kinetic energy (m^2/s^2)

K_A, K_V mass concentration of air and vapor in binary vapor–air mixture

K_{VS} mass concentration of vapor at the droplet surface an evaporating corresponding to saturation parameters at the droplet temperature T_L

L heat of vaporization (J/kg)

$Le = Pr/Sc$ Lewis number

$m = \rho_S U_S/\rho_0 U_0$ blowing parameter

M_A, M_V, M_L air, vapor, and liquid mass concentration in the triple air–vapor–liquid mixture

$Nu_L = \alpha d/\lambda$ droplet Nusselt number

$Nu_P = \alpha_P d_P/\lambda$ Nusselt number non-evaporating particle

P pressure (N/m^2)

$Pr = C_p\mu/\lambda$, Prandtl number

$\Re$ absolute gas constant, (J/kg K)

R tube radius (m)

$Re_J = Jd/\mu$ Reynolds number calculated from the mass rate of the vapor flow from the surface of an evaporating droplet

$Re_L = \rho d\sqrt{(U-U_L)^2 + (V-V_L)^2}/\mu$ Reynolds number of disperse phase

$Re_T = k^2/\varepsilon\nu$ turbulence Reynolds number

S slot height (m)

U, V velocity component in axial and radial directions (m/s)

$\langle uv\rangle = -\nu_T \frac{\partial U}{\partial r}$ turbulent stresses in gas phase (m^2/s^2)

$\langle u_L v_L\rangle$ correlations between the longitudinal and transverse pulsating velocities of liquid droplets (m^2/s^2)

$\langle u^2\rangle$, $\langle v^2\rangle$ root-mean-square velocity fluctuations in axial and radial directions (m^2/s^2)

U_* wall friction velocity (m/s)

$Sc = \nu/D$ Schmidt number

$Sh = \beta d/D$ Sherwood number

$St_D = -\rho_V D \frac{\partial K_{VS}}{\partial r}/\rho U(K_{VS} - K_V)$ diffusional Stanton number

T temperature (K)

$\langle tv\rangle = -\frac{\nu_T}{Pr_T}\frac{\partial T}{\partial r}$ turbulent heat flux in gas phase (Km/s)

Tu turbulence intensity in the flow

V_{LW} droplet deposition velocity (m/s)

$W = (1 + Re_L^{2/3}/6)$ correction factor for the Stokes law

$We = \rho \mid \vec{U} - \vec{U}_L \mid d_1/\chi$ Weber number

x_0 initial region length of near-wall screen, where $\Theta_T = 1$ (m)

y coordinate normal to the wall (m)

$y_\lambda = y/\sqrt{\nu k/\tilde{\varepsilon}}$ Taylor microscale

Greek symbols

α heat transfer coefficient (W/m^2 K)

β mass transfer coefficient (m/s)

δ thickness of the boundary layer (m)

$\varepsilon = \tilde{\varepsilon} + \hat{\varepsilon}$ dissipation rate (m^2/s^3)

$\tilde{\varepsilon}$ dissipation rate (m^2/s^3)

$\hat{\varepsilon} = 2\mu/\rho[\partial(\sqrt{k})/\partial r]^2$ rate of energy dissipation in the near-wall zone ($y_+ \leqslant 15$) (m^2/s^3)

Φ volume mass concentration of droplets

$\Gamma^E = \nu_T/\langle u^2\rangle$ turbulence scale of gas phase (m)

ϕ humidity of the flow

λ thermal conductivity (W/m K)

μ dynamic viscosity (N s/m^2)

ν kinematic viscosity (m^2/s)

$\Theta_T = (T_0 - T_W)/(T_0 - T_S)$ relative thermal efficiency profile

$\langle \theta v_L\rangle$ correlation between the droplet-temperature fluctuations and droplet-velocity fluctuations (Km/s)

$\Omega^\varepsilon = (15\nu/\varepsilon)^{1/2}$ time microscale (s)

Ω^E Eulerian time macroscale (s)

Ω^L Lagrangian time macroscale (s)

$\Omega^{\varepsilon L}$ time of particle interaction with the intense vortices (s)

$\Omega_{\theta u}$ time of droplet contact with intense gas-temperature pulsations (s)

ρ, ρ_L, ρ_V mixture, liquid, vapor densities (kg/m^3)

χ surface tension (N/m^2)

$\tau = \rho_L d^2/18\mu W$ particle relaxation time (s)

$\tau_\Theta = C_{pL}\rho_L d^2/(6\lambda Nu_L)$ particle thermal relaxation time (s)
$\xi = \frac{x}{mS}(\mu_S Re_S/\mu_0)^{-0.25}$ parameter

Subscripts

0	parameter at the main flow
1	parameter under inlet conditions
A	air
D	diffusional parameter
i	current calculation cross-section along the axial direction
$i-1$	previous calculation cross-section along the axial direction
L	droplet
P	non-evaporating particle
S	parameter at the secondary flow
T	turbulent parameter
V	vapor
W	parameter under condition at the adiabatic wall
+	denotes the dimensionless variables in dynamic universal units

mixing-length theory [5]. The authors of [1–6] considered the case of single-phase turbulent boundary layers with gas screens organized on an adiabatic, a non-adiabatic, or on a reacting surface. Simple design formulas were derived to predict the thermal efficiency of wall screens. Many experimental and numerical data were reported concerning the spreading pattern of single-phase near-wall flows. Various methods for organizing wall jets were considered, including porous blowing, injection through tangential slots, blowing through stepped constructions, and injection of inert or reacting gases.

The organization of two-phase gas-droplet wall screens offers a most promising way for raising the screen efficiency. The main mechanism underlying good protective properties of two-phase gas-droplet systems consists in utilizing the phase change heat in the immediate neighborhood of the wall. Previous experimental and numerical studies ([7–16]) proved it possible to obtain a 50–100% gain in the screen efficiency by using gas-droplet wall screens.

The use of two-phase coolants in technical apparatuses is seriously impeded by the lack of reliable simulation data for two-phase flows. Here one meets a very complex problem whose statement involves too many factors to be taken into account. The involvement of the liquid phase in the problem and its boundary layer evaporation necessitates taking into account the interphase heat, mass and momentum transfer. Moreover, the presence of the second gas phase component, e.g., air mixed to water vapor, makes the solution of the problem rather difficult since there arises a necessity in joint solution of energy and diffusion equations for the vapor–gas mixture.

Presently, the numerical studies of two-component gas-droplet screens performed with the use of integral approaches are few in number (see, for instance, [8–11]). Available publications fall into two groups:

1. Models based on the analogy between heat and mass transfer [8,9,11].
2. The "evaporation front" model [10].

The model was developed in papers [8,9,11] can be further subdivided into equilibrium models [8] (wherein the temperatures of the two phases are assumed identical, equal to the adiabatic evaporation temperature) and non-equilibrium models [9,11] (when the temperatures of the two phases are assumed different). In particular, calculations according to these models boil to solving the energy equation written as an expression for the mean dimensionless temperature in the current cross-section of the two-phase boundary layer. The relations for screen efficiency can be obtained from the condition of similarity between vapor concentrations and temperatures or from the similarity between the concentration fields of components in the two-phase mixture and the fields of total enthalpies in the gas–vapor–liquid flow. The thermal, dynamic, and diffusion boundary layers here are assumed to have identical thickness. The fact is taken into account that the mass concentration of the vapor in the calculation cross-section is determined not only by mass mixing of the mainstream and secondary flows, but also by the increase in the mass of vapor due to liquid evaporation from the drop surface. Both approaches yield similar results.

The second approach, developed in [10], treats a planar turbulent boundary layer developing on an adiabatic wall behind the point of injection. Differential energy and diffusion equations were solved by the integral method with invoking the Reynolds analogy. To predict the distributions of temperatures and concentrations, the diffusion combustion front model was used [17]. The basic limiting integral of the asymptotic theory of turbulent boundary layer was divided into two parts: from the wall to the evaporation front (two-phase zone) and from the front to the outer border of the wall jet (single-phase zone). The evaporation rate was assumed to be infinitely high. Heat transfer and mass transfer in the boundary layer both were assumed conditioned by diffusion transfer. The evaporation front is impermeable to the liquid phase, and the front contains only the saturated gas–vapor mixture. The vapor diffuses from the front region to the outer border of the boundary layer. In this work, a

relation for the thermal-protection efficiency of adiabatic wall with blowing of a two-phase coolant is proposed, which agrees rather well with experimental data and allows one to predict the characteristics of the screen in its single-phase and two-phase parts.

Available integral theoretical approaches, developed in a series of works, employ a number of simplifying assumptions that still require detailed substantiation. Models constructed around sets of differential boundary layer equations for two-component two-phase mixtures are devoid of many such drawbacks ([13,14,16]). Such models make it possible to take into account specific features of heat and mass transfer processes in gas-droplet wall jets in a more rigorous formulation. The present study is a continuation of our previous works [13,14,16] aimed at development of mathematical models for complex gas-droplet flows with phase transitions.

A calculation model is developed in papers [13,14] and numerical investigation performed of the heat and mass transfer characteristics in a turbulent gas-droplet near-wall screen. The model is based on the system of transfer equation written in the boundary-layer approximation. To close the system, the two-layer algebraic model of turbulence was used. It was assumed that the disperse phase exerts no influence on gas turbulence. Of course, this assumption is valid only if the drop concentration is low and the drop size is small. The case of small parameters of injection $m = \rho_S U_S/\rho_0 U_0 < 1$ was investigated, where the prevailing part in the process of wall jet development is played by the regularities of wall turbulence [1]. The subscripts "S" and "0" indicate the parameters of the secondary and main flows, respectively. The effect of the characteristics of a two-phase vapor–gas-droplet flow on the thermal efficiency is analyzed. The evaporation of droplets in a two-phase wall screen brings about a significant improvement in the protective properties of an adiabatic wall compared with a single-phase flow mode. The results of calculations of two-phase cooling are compared with experimental data.

In such a formulation, we solve the heat and mass transfer problem for a wall jet developing in a cocurrent gas flow. In the present formulation, the wall is assumed adiabatic; therefore, primary attention in the present study was concentrated on studying effects of various factors (liquid phase content of the mixture, injection parameters, flow nonisothermality, and droplet diameter) on the variation of the adiabatic wall temperature, which directly defines the efficiency of a two-phase gas-droplet wall screen.

2. Formulation of the problem

The flow diagram of the wall jet flow is shown in Fig. 1. Here S—slot height; δ—the boundary layer thickness.

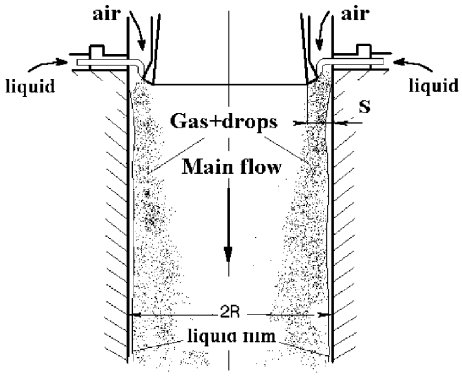

Fig. 1. The scheme of the gas-droplets near-wall screen in a tube.

The present statement of the problem is based on using the set of Eulerian–Eulerian two-fluid model [19–24], written both for the gaseous phase and for the particles within the framework of the two-liquid model of transport processes in the gas and dispersed phases. This set of equations takes into account the effect of turbulence-induced droplet migration on the rate of heat and mass transfer between the gas flow and the liquid droplets, the force due to turbophoresis, and the diffusion of particles due to gradients of their concentration. On the whole, the equations for the averaged flow velocity and for the root-mean-square fluctuations of the dispersed phase velocity answer the model used in [25]. To close the set of transfer equations for the gas phase, the k–$\tilde{\varepsilon}$ model of turbulence was used [24].

We consider a gas-droplet wall jet injected into a piped single phase turbulent flow of hot air with allowance for droplet evaporation, interaction between the phases, deposition of particles onto the wall, heat transfer with the wall, turbulent migration of the particles, turbophoresis, and vapor diffusion into the vapor–gas mixture. Both the wall jet and the main stream are downward flows. The main assumptions in the present study are the same as in Terekhov and Pakhomov [16,18]. The volume concentration of the liquid phase is low ($\Phi < 10^{-4}$), and the liquid droplets are fine (droplet diameter $d_l < 100$ μm). In the flow, the droplets do not coalesce (because the dispersed phase content is low), and no droplet fragmentation occurs (the Weber number $We = (\vec{U} - \vec{U}_L)d/\chi$ constructed on the droplet diameter and on the slip velocity of the phases is well below unity). According to Volkov et al. [19], in the case of two-phase flows, the collisions between particles can be disregarded if $\Phi < 0.1\%$. The droplets are shaped as spheres with stationary boundaries. The adiabatic wall is assumed to always remain dry because the droplets, as they come into contact with the wall, undergo instantaneous evaporation. The particle concentration permanently decreases in the downstream direction because of

droplet deposition onto channel walls and jet flow expansion. The droplet diameter is assumed to vary both along and across the pipe because the evaporation intensity is spatially variable, dependent on the local gas phase temperature. The temperature of an individual droplet along its radius is assumed constant.

A comparison of numerical results with experimental data for the case of turbulent airflow with evaporating liquid drops was reported in [29]. In this study, a comparison between numerical and experimental results was also made for gas flows with solid particles and no heat exchange with the channel wall.

3. The system of governing equations

3.1. Gas phase

Under the adopted assumptions, the set of equations including the continuity equation, the equation of axial motion, the energy equation, and the equation of diffusion of vapor to the binary vapor–gas mixture for an axisymmetric two-phase gas-droplet flow in the boundary layer approximation has the form

$$U\frac{\partial U}{\partial x}+\frac{1}{r}\frac{\partial(rV)}{\partial r}=\frac{6J\Phi}{\rho d}$$

$$\rho\left[U\frac{\partial U}{\partial x}+\frac{V}{r}\frac{\partial(rU)}{\partial r}\right]=-\frac{\partial P}{\partial x}+\frac{\rho}{r}\frac{\partial}{\partial r}\left[r(\mu+\mu_{\mathrm{T}})\frac{\partial U}{\partial r}\right]-\frac{\Phi(U-U_{\mathrm{L}})}{d}\left[\frac{3}{4}C_{\mathrm{D}}\rho\mid\vec{U}-\vec{U}_{\mathrm{L}}\mid+6J\right]\pm\rho g$$

$$\rho C_{\mathrm{p}}\left[U\frac{\partial T}{\partial x}+\frac{V}{r}\frac{\partial(rT)}{\partial r}\right]=\frac{1}{r}\frac{\partial}{\partial r}\left[r\left(\frac{\mu}{Pr}+\frac{\mu_{\mathrm{T}}}{Pr_{\mathrm{T}}}\right)\frac{\partial T}{\partial r}\right]-\frac{\alpha}{d}(T-T_{\mathrm{L}})+\rho D_{\mathrm{T}}\frac{\partial K_{\mathrm{V}}}{\partial r}(C_{\mathrm{pV}}-C_{\mathrm{pA}})\frac{\partial T}{\partial r}$$

$$\rho\left[U\frac{\partial K_{\mathrm{V}}}{\partial x}+\frac{V}{r}\frac{\partial(rK_{\mathrm{V}})}{\partial r}\right]=\frac{1}{r}\frac{\partial}{\partial r}\left[r\left(\frac{\mu}{Sc}+\frac{\mu_{\mathrm{T}}}{Sc_{\mathrm{T}}}\right)\frac{\partial K_{\mathrm{V}}}{\partial r}\right]+\frac{J\Phi}{d}$$

$$\rho=P/(\Re T);\quad \partial P/\partial r=0, \tag{1}$$

where C_{p}—heat capacity of the gas–vapor mixture; D_{T}—coefficient of vapor diffusivity in vapor–air mixture; d—droplet diameter; $\partial P/\partial x$—longitudinal pressure gradient.

The continuity, energy, and diffusion equations contain source and sink terms that model the effect of liquid droplets on transport processes, and the equation of motion involves an additional term that takes into account the dynamic interaction between the phases.

At the initial section of the pipe, the relation for determining the derivative $\partial P/\partial x$, which appears in the equation of motion, is represented by the Bernoulli integral with allowance for the additional inflow of vapor mass due to droplet evaporation.

3.2. Two-equation k–$\tilde{\varepsilon}$ model of turbulence

The equations for the kinetic turbulence energy k and for the dissipation rate of this energy $\tilde{\varepsilon}$, modified so that to cover the case of a dispersed phase present in the flow, have the form

$$\rho\left[U\frac{\partial k}{\partial x}+\frac{V}{r}\frac{\partial(rk)}{\partial r}\right]=\frac{\rho}{r}\frac{\partial}{\partial r}\left[r\left(\mu+\frac{\mu_{\mathrm{T}}}{\sigma_k}\right)\frac{\partial k}{\partial r}\right]+\Pi-\rho\varepsilon+\Pi_k+S_k$$

$$\rho\left[U\frac{\partial\tilde{\varepsilon}}{\partial x}+\frac{V}{r}\frac{\partial(r\tilde{\varepsilon})}{\partial r}\right]=\frac{\rho}{r}\frac{\partial}{\partial r}\left[r\left(\mu+\frac{\mu_{\mathrm{T}}}{\sigma_\varepsilon}\right)\frac{\partial\tilde{\varepsilon}}{\partial r}\right]+\frac{C_{\varepsilon1}\tilde{\varepsilon}f_1\Pi}{k}-\frac{C_{\varepsilon2}\tilde{\varepsilon}^2\rho f_2}{f_2 k}+\frac{C_{\varepsilon3}}{4}\frac{k^2}{\tilde{\varepsilon}}\frac{\partial U}{\partial x}\left(\frac{V}{r}\right)^2+\Pi_\varepsilon+S_\varepsilon$$

$$\mu_{\mathrm{T}}=C_\mu f_\mu\rho k^2/\tilde{\varepsilon}. \tag{2}$$

The constants and the damping functions are as follows [26]:

$$C_\mu=0.09;\quad \sigma_k=1.4-1.1\exp[-(0.1y_\lambda)];\quad C_{\varepsilon1}=1.44;\quad C_{\varepsilon2}=1.92;\quad \sigma_\varepsilon=1.3-\exp[-(0.1y_\lambda)];$$

$$f_\mu=1-\exp(-0.01y_\lambda-0.008y_\lambda^3);\quad \Pi=\mu_{\mathrm{T}}\left(\frac{\partial U}{\partial r}\right)^2;$$

$$f_1=f_2=1;\quad \Pi_k=-\frac{\mu}{2}\frac{\partial}{\partial r}\left(\frac{k}{\varepsilon}\frac{\partial\hat{\varepsilon}}{\partial r}\right);$$

$$\Pi_\varepsilon=-\frac{\mu}{r}\frac{\partial}{\partial r}\left(r\frac{\varepsilon}{k}\frac{\partial k}{\partial r}\right).$$

The coefficient $C_{\varepsilon3}=0.79$, which takes into account the deformation of turbulent eddies in the internal flow, is borrowed from the well-known model by Jones and Lounder [27]; $\varepsilon=\tilde{\varepsilon}+\hat{\varepsilon}$; In the flow core (for $y_+>15$), the parameter $\hat{\varepsilon}$ is assumed to be zero. The coefficient $C_{\varepsilon3}=0.79$, which takes into account the deformation of turbulent eddies in the internal flow, is borrowed from the well-known model by Jones and Lounder [27].

The components defining the additional dissipation of gas-phase turbulence energy by fine droplets and the exchange with energy with the averaged motion due to the averaged slipping in the flow with nonuniformly distributed droplets have the form [19,28]

$$S_k=-\frac{2M_{\mathrm{L}}\rho k}{\tau}\exp(-\Omega^{\mathrm{L}}/\tau)-g_k\mu_{\mathrm{T}}(U-U_{\mathrm{L}})\frac{\partial U}{\partial x}\frac{\partial M_{\mathrm{L}}}{\partial x}-\frac{6kJ\Phi}{d}\left(1-\frac{\Omega^{\mathrm{L}}}{\Omega^{\mathrm{L}}+\tau}\right). \tag{3}$$

The effect of fine droplets on the rate of dissipation of the flow-carrier turbulence energy, and the backward

effect on the turbulence due to averaged slipping and due to nonuniform distribution of the dispersed phase, are given by the following relation [19,28]:

$$S_\varepsilon = -\frac{2M_L\rho_L\widetilde{\varepsilon}}{\tau}\exp(-\Omega^\varepsilon/\tau) - \frac{2}{3}g_\varepsilon\rho\widetilde{\varepsilon}\left[(U-U_L)\frac{\partial M_L}{\partial x}+(V-V_L)\frac{\partial M_L}{\partial r}\right] - \frac{6\widetilde{\varepsilon}J\Phi}{d}\left(1-\frac{\Omega^L}{\Omega^L+\tau}\right), \quad (4)$$

where $\Omega^\varepsilon = (15\nu/\varepsilon)^{1/2}$—Eulerian micro-time scale of turbulence; $\Omega^{\varepsilon L}$—time of droplet interaction with intense eddies; Ω^L—Lagrangian time turbulence macroscale. The last terms in S_k and S_ε stand to allow for the effect of droplet evaporation on the gas phase turbulence structure [18,19]. The coefficients of particle involvement into the micropulsational motion of the gas flow are [18,19]

$$g_k = \Omega^{\varepsilon L}/\tau - 1 + \exp(-\Omega^{\varepsilon L}/\tau);$$
$$g_\varepsilon = \Omega^\varepsilon/\tau - 1 + \exp(-\Omega^\varepsilon/\tau).$$

The turbulent Prandtl and Schmidt numbers, $Pr_T = Sc_T = 0.9$, are assumed to be uniform both along and across the pipe. The Lewis number is $Le = Pr/Sc = 1$.

3.3. Dispersed phase

3.3.1. Momentum and energy equations for the droplets

Numerous reported studies prove that the main forces acting on a particle in a turbulent flow under the conditions of interest are the aerodynamic drag, the gravity force, and the turbophoresis.

The set of equations that includes the continuity equation for the dispersed flow, the axial-velocity equation in the axial and radial directions, and the equation of continuity in the cylindrical coordinate system, has the form [25]

$$\frac{\partial(\Phi U_L)}{\partial x}+\frac{1}{r}\frac{\partial(r\Phi V_L)}{\partial r} = -\frac{6J\Phi}{\rho_L d}$$

$$U_L\frac{\partial U_L}{\partial x}+\frac{V_L}{r}\frac{\partial(rU_L)}{\partial r}+\frac{\partial\langle v_L^2\rangle}{\partial x}+\frac{1}{r\Phi}\frac{\partial}{\partial r}[r\Phi\langle u_L v_L\rangle] = \frac{U-U_L\pm\tau g}{\tau}-\frac{D_{xL}}{\tau}\frac{\partial\ln\Phi}{\partial r}$$

$$U_L\frac{\partial V_L}{\partial x}+\frac{V_L}{r}\frac{\partial(rV_L)}{\partial r}+\frac{\partial\langle v_L^2\rangle}{\partial r} = \frac{V-V_L}{\tau}-\frac{D_{rL}}{\tau}\frac{\partial\ln\Phi}{\partial r}. \quad (5)$$

The quantities $\langle u_L v_L\rangle$, which represent correlations between the fluctuations longitudinal velocity and the pulsational transverse velocities of the particles and, simultaneously, turbulent stresses in the dispersed phase, are written as [25]

$$\langle u_L v_L\rangle = q_L\langle uv\rangle - \frac{1}{2}\tau\langle v_L^2\rangle\frac{\partial U_L}{\partial r};\quad q_L = 1-\exp(-\Omega^{\varepsilon L}/\tau);$$

$$p_L = \Omega^{\varepsilon L}/\tau - q_L;\quad D_{xL} = \tau(\langle u_L^2\rangle + p_L\langle u^2\rangle);$$
$$D_{rL} = \tau(\langle v_L^2\rangle + p_L\langle v^2\rangle). \quad (6)$$

The energy equation for the averaged droplet temperature T_L is [25]

$$U_L\frac{\partial T_L}{\partial x}+\frac{V_L}{r}\frac{\partial(rT_L)}{\partial r}+\frac{1}{r\Phi}\frac{\partial}{\partial r}(r\Phi\langle\theta v_L\rangle) = \frac{6}{C_{pL}\rho_L d}\{\alpha(T-T_L)-J[L+C_{pV}(T-T_L)]\}, \quad (7)$$

where $\langle\theta v_L\rangle$ is the correlation between the droplet temperature fluctuations and droplet velocity pulsations [25]

$$\langle\theta v_L\rangle = f_{\theta v}\langle tv\rangle - \left(\frac{1}{\tau}-\frac{1}{\tau_\Theta}\right)^{-1}\langle v_L^2\rangle\frac{\partial T_L}{\partial r}.$$

Here t is the amplitude of gas-temperature pulsations and $f_{\theta v}$ is the function that describes the entrainment of liquid drops into the intense pulsations of the gas-phase velocity and the gas-phase temperature

$$f_{\theta v} = \{\tau[1-\exp(-\Omega_{\theta u}/\tau)] + \tau_\Theta[1-\exp(-\Omega_{\theta u}/\tau_\Theta)]\}(\tau+\tau_\Theta)^{-1}.$$

Here $\Omega_{\theta u}$- time of droplet interaction with intense gas temperature fluctuations.

3.3.2. Equations for the pulsating dispersed-phase velocity

The equations for the second moments of turbulent fluctuations of the droplet velocity in the longitudinal and transverse directions can be found in [25]:

$$U_L\frac{\partial\langle u_L^2\rangle}{\partial x}+\frac{V_L}{r}\frac{\partial(r\langle u_L^2\rangle)}{\partial r}+\frac{1}{r\Phi}\frac{\partial}{\partial r}\left[\frac{\partial(r\Phi\langle u_L^2 v_L\rangle)}{\partial r}\right] + 2\langle u_L^2\rangle\frac{\partial U_L}{\partial x} = \frac{2}{\tau}(q_L\langle u^2\rangle-\langle u_L^2\rangle)$$

$$U_L\frac{\partial\langle v_L^2\rangle}{\partial x}+\frac{V_L}{r}\frac{\partial(r\langle v_L^2\rangle)}{\partial r}+\frac{1}{r\Phi}\frac{\partial}{\partial r}\left[\frac{\partial(r\Phi\langle v_L^3\rangle)}{\partial r}\right] = \frac{2}{\tau}(q_L\langle v^2\rangle-\langle v_L^2\rangle). \quad (8)$$

3.3.3. Friction, and heat and mass transfer, for the single evaporating droplet

For evaporating droplets, the drag coefficient C_D is [29]:

$$C_D = \frac{C_{DP}}{1+C_p(T-T_L)/L}. \quad (9)$$

Here C_{DP} is the drag coefficient of non-evaporating droplets. It is determines on the quantities for solid particles in Volkov et al. [19].

$$C_{DP} = \begin{cases} 24/Re_L, & Re_L \leqslant 1 \\ \dfrac{24}{Re_L}(1 + Re_L^{2/3}/6), & Re_L > 1, \end{cases} \quad (10)$$

where $Re_L = (\vec{U} - \vec{U}_L)d/\nu$—droplet Reynolds number.

The equation of vapor–mass conservation on the evaporating droplet surface is

$$J = JK_{VS} - \rho_V D\left(\frac{\partial K_V}{\partial r}\right)_{drop}. \quad (11)$$

Expression (11) finally assumes the form [13]

$$J = Sh_L \rho(\vec{U} - \vec{U}_L) b_{1D}/(Re_L Sc). \quad (12)$$

Here b_{1D} is diffusional injection parameter for the vapor released by an evaporation.

Within the framework of the "film model", the effect of the transverse inflow of mass on the heat- and mass transfer coefficients of evaporating droplets are given by the relations used in [19].

$$Nu_L = \frac{Re_J Pr}{\exp(Re_J Pr/Nu_P) - 1};$$
$$Sh_L = \frac{Re_J Pr}{\exp(Re_J Pr/Sh_P) - 1}, \quad (13)$$

$$Nu_P = \alpha_P d/\lambda = 2 + 0.6 Re_L^{1/2} Pr^{1/3};$$
$$Sh_L = \beta d/D = 2 + 0.6 Re_L^{1/2} Sc^{1/3}. \quad (14)$$

Here Sh—Sherwood number; Sc—Schmidt number.

3.4. Determination of the intensity of gas-phase pulsations

To perform a comparison of numerical results with experimental data on the components of gas-phase velocity pulsations and droplet velocity pulsations, it was necessary to calculate these quantities. It was assumed that the droplets are relatively large, so that the dynamic time τ of their relaxation is longer than the integral Euler time scale Ω^E of the turbulence.

The time macroscale of the flow core turbulence was calculated from the relation borrowed from the work of Simonin et al. [30]:

$$(\Omega^E)_0 = 0.22 k/\varepsilon.$$

Near the duct wall, the integral Euler time scale of the turbulence, needed for determining the transverse component of gas-phase pulsations, was approximated by the following relation [23]:

$$\Omega_+^E = \Omega^E U_* / \nu = \sqrt{(\Omega_+^E)_0^2 + (\Omega_+^E)_W^2}; \quad (\Omega_+^E)_W \approx 10.$$

The radial component of the root-mean-square gas-phase velocity pulsations is related with the turbulent diffusivity:

$$\langle v^2 \rangle = \nu_T / \Omega^L.$$

The amplitude of gas-phase velocity pulsations in the axial direction was calculated by the following formula [25]:

$$\langle u^2 \rangle \approx 1.3k,$$

and the relation between the time scales of turbulence for the case of small particles has the form

$$\Omega^L \approx 0.608 \Omega^E.$$

4. Boundary conditions

At the pipe axis, the following symmetry conditions are set:

$$\frac{\partial T}{\partial r} = \frac{\partial K_V}{\partial r} = \frac{\partial U}{\partial r} = V = \frac{\partial U_L}{\partial r} = V_L$$
$$= \frac{\partial \langle u_L^2 \rangle}{\partial r} = \frac{\partial \langle v_L^2 \rangle}{\partial r} = \frac{\partial T_L}{\partial r} = \frac{\partial k}{\partial r} = \frac{\partial \widetilde{\varepsilon}}{\partial r} = 0. \quad (15)$$

At the channel wall, the no-slip condition for the gas phase velocity and the condition of wall impermeability are adopted; for the heat flow, the boundary condition on an adiabatic wall disregarding the droplets deposited onto the wall from the two-phase flow is used:

$$U = V = \frac{\partial K_V}{\partial r} = 0; \quad \frac{\partial T}{\partial r} = 0; \quad k = \widetilde{\varepsilon} = 0. \quad (16)$$

For the dispersed phase, the boundary conditions for the squared pulsations of the axial and radial velocities, and for the squared fluctuations of temperature, have the form [25]

$$\langle v_L^2 \rangle \frac{\partial U_L}{\partial r} = -\frac{2}{\tau} q_L \nu_T \left(\frac{\partial U}{\partial r}\right)_W; \quad V_{LW} = \left(\frac{2}{\pi}\langle v_L^2 \rangle\right)^{1/2};$$
$$\frac{\partial \langle u_L^2 \rangle}{\partial r} = 0; \quad \frac{\partial \langle v \rangle}{\partial r} = -V/\tau;$$
$$\frac{\langle v_L^2 \rangle}{(1/\tau - 1/\tau_\Theta)} \frac{\partial T_L}{\partial r} = -f_{\theta v} \frac{\nu_T}{Pr} \frac{\partial T}{\partial r}. \quad (17)$$

We assume that the droplets deposited onto the wall never return into the flow and do not affect the heat transfer with the channel wall.

In the inlet cross-section of the pipe, the temperatures and velocities of the phases are spatially uniform. For the main, single-phase flow ($0 \leqslant r \leqslant (R - S)$), we assume that

$$U = U_0; \quad V = V_0; \quad T = T_0; \quad K_V = K_{V1};$$
$$k_0 = k_{01}; \quad \widetilde{\varepsilon} = \widetilde{\varepsilon}_{01}. \quad (18)$$

For the two-phase gas-droplet jet ($(R - S) \leqslant r \leqslant R$), we assume that

$$U = U_{SL}U_S; \quad V = V_{SL} = V_S; \quad T = T_{SL} = T_1;$$
$$M_L = M_{L1}; \quad d = d_1; \quad K_V = K_{V1}; \quad k = k_{S1}; \quad \widetilde{\varepsilon} = \widetilde{\varepsilon}_{01}. \tag{19}$$

Here V_{LW}—deposition velocity; subscript "1" is the initial parameter.

For uniform inlet profiles of the turbulent energy k and for the rate of its dissipation $\widetilde{\varepsilon}$, the data of [31] were used. In the study, the turbulence level of the gas phase at the channel inlet is adopted to be $Tu_{01} = 4\%$ in the mainstream flow and $Tu_{S1} = 7\%$ in the near-wall flow. All droplets at the channel inlet are the same size and temperature. The temperatures of the phases at the nozzle exit plane are identical (homogeneous).

5. Numerical realization

The numerical solution of the parabolic-type partial differential equations was obtained by the Crank–Nickolson finite-difference scheme, by way of transforming the set of initial partial differential equations into a set of discrete linear algebraic equations; a detailed description of this scheme can be found in Anderson et al. [32]. The system obtained, with a three-diagonal matrix, was solved by the sweep method using the Thomas algorithm, described in more details in [32]. In the radial direction, a logarithmically nonuniform calculation grid was used. In the radial direction, a logarithmically nonuniform calculation grid was used. This was achieved using the stretching scheme suggested in [33]. That is

$$y_{comp} = 1 - \frac{\ln\{[\varpi + 1 - y/R]/[\varpi - 1 + y/R]\}}{\ln[(\varpi + 1)/(\varpi - 1)]}, \tag{20}$$

where $\varpi = 1.03$ is the stretching parameter.

The distance between the next to the wall calculation point and the wall was $y_+ = 1$. In the axial direction, the grid was uniform.

The distance between the first calculation point and the wall was $y_+ = yU_*/\nu = 1.5$. In the axial direction, the grid was uniform.

All calculations were performed on a grid containing a total of 201 nodal points in the axial direction and 101 nodal points in the axial direction. Preliminary methodical calculations were performed on a finer, 201×201 nested grid. Further increase in the number of nodal points was found to induce no changes in the calculation results.

Since system (1)–(19) contains nonlinear equations, an iteration algorithm was used to solve it. In this procedure, the following convergence criteria were used: $|Y_k - Y_{k-1}| < 10^{-4}$, where Y stand for U, k, $\widetilde{\varepsilon}$, T, K_V, U_L, V_L, $\langle u_L^2\rangle$; $\langle v_L^2\rangle$, and T_L, and the subscript k enumerates the iterations. The calculations were terminated as soon as all of the above criteria were fulfilled.

6. The testing of the numerical model

The predicted evolution of velocity profiles in the gas wall screen along the channel length is shown in Fig. 2. These profiles are compared with the experimental data obtained by Sharov and Shishkin. One can observe a fairly good agreement between the experimental and numerical data in the near-wall zone.

The present computational model was verified through comparison of predicted values with available theoretical and experimental data for single-phase wall gas screens. The results are shown in Fig. 2. The thermal efficiency of a wall gas screen was defined as a dimensionless complex reflecting the lengthwise variation of adiabatic wall temperature [1–5]. This complex was considered as a function of another dimensionless complex, $\xi = \frac{x}{mS}(\mu_S Re_S/\mu_0)^{-1/4}$, used in the theory of single-phase gas screens. In the above complexes, x is the longitudinal coordinate; $m = \rho_S U_S/\rho_0 U_0$ is the injection ratio; $Re_S = U_S S/\nu_S$ is the Reynolds number constructed on secondary-flow characteristics. The points show the experimental data by [4]. Curves 1 and 2 are theoretical dependences calculated by the formulas proposed by Goldstein [2] and Kutateladze and Leont'ev, [1], respectively. It follows from Fig. 2 that, on the whole, the predicted thermal efficiency Θ_T well agrees with the data calculated by available integral algorithms and with experimental data, thus validating the main assumptions underlying the present computational model.

In the Fig. 3 are shown the data on influence of blowing parameter U_S/U_0 on efficiency of screen cooling. Solid curves are the calculation by theoretical formulas [4] for quasi isothermal screen ($\rho_0 \approx \rho_S$):

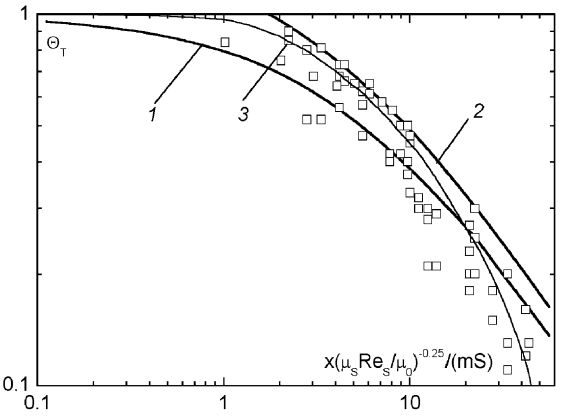

Fig. 2. Efficiency of gas wall screen in the single-phase flow mode. The points here are the experimental data borrowed from [4]. Curves 1 and 2 were calculated by the Goldstein formula [2] $\Theta_T = 1.9Pr^{2/3}/(1 + 0.329\xi^{0.8})$ and by the Kutateladze–Leont'ev formula $\Theta_T = (1 + 0.249\xi)^{-0.8}$ [1] and curve 3 shows the data calculated by the present model.

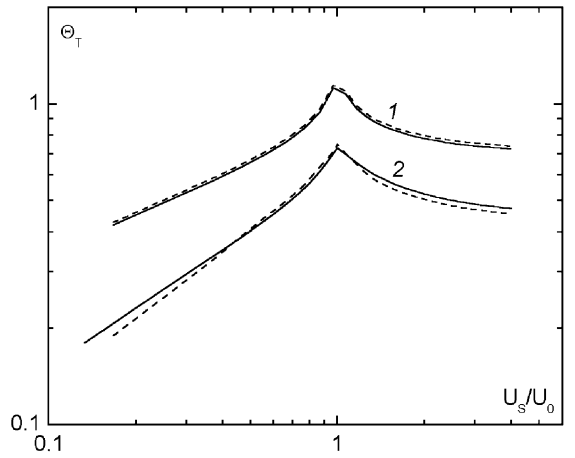

Fig. 3. Effect of blowing parameter m on the efficiency of single-phase gas screen. 1—$A = 1$, 2—$A = 5$. Solid curves—calculation by formula (21); dashed curves—data obtained in the present study.

$$\Theta_T = \frac{\left[(1 + 62.5/A)(1 + 62.5 \mid 1 - U_S/U_0|^{1.25}) - 1\right]^{0.8}}{(1 + 0.016A)^{0.16}}. \tag{21}$$

It is seen, the maximal value of thermal efficiency is reached at equality of velocities of the main and second streams $U_S/U_0 = 1$. The value Θ_T is also reduced with decrease of blowing parameter $U_S/U_0 < 1$. The effectiveness reduction with $U_S/U_0 > 1$ is not very intensive and with the big blowing parameter the quantity is asymptotic. It is noted, that a fairly good agreement between the numerical simulation data and theoretical formulas proposed by [4] for one-phase isothermal screen both for $U_S/U_0 < 1$ and for $U_S/U_0 > 1$.

7. Numerical results and its discussion

7.1. Profiles of parameters of gas-droplets screen

The evolution of the longitudinal velocity for two values of the injection parameter, $m = 0.8$ and $m = 1.5$, is shown in Fig. 4 (a) and (b), respectively. At large distances from the slot plane, a flow that displays regularities typical of the single-phase flow is observed [1]. These properties of the flow under study are observed both for $m < 1$ and for $m > 1$. This fact can be explained by the fact that the majority of droplets undergo evaporation and by completion of jet mixing in the channel between the wall jet and the mainstream flow. At higher blowing parameter, when a jet with a velocity greater than the mainstream flow velocity develops in the near-wall region, restoration of the flow to a developed turbulent flow is observed, as it follows from Fig. 4b,

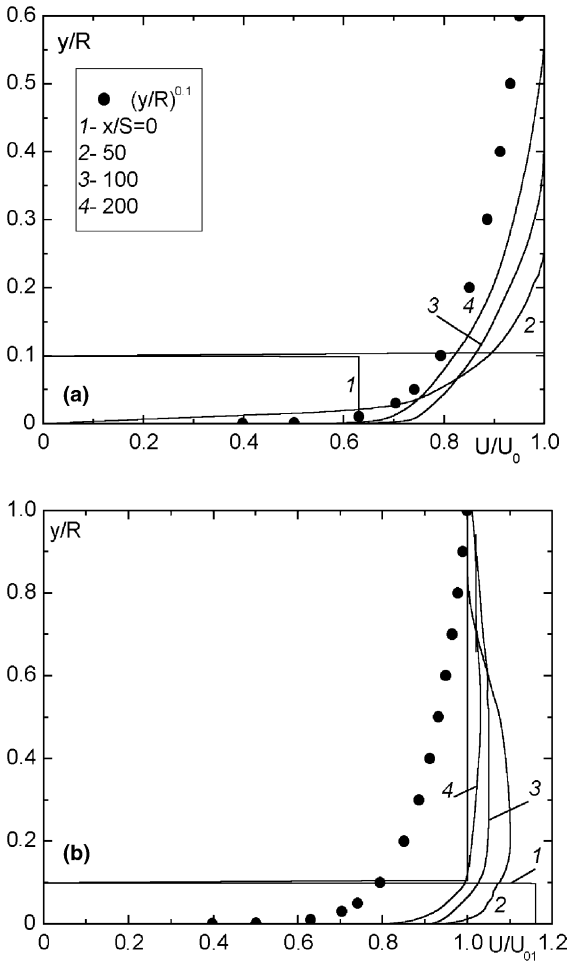

Fig. 4. The gas phase profiles of gas-droplets jet with various injection parameters. $T_0 = 373$ K; $T_S = T_{L1} = 293$ K; $d = 30\,\mu$m; $M_{L1} = 0.05$. (a)—$m = 0.8$; (b)—$m = 1.5$. 1—$x/S = 0$; 2—50; 3—100; 4—200.

over larger distances from the slot exit plane compared to the case of $m < 1$.

The complex heat and mass transfer regularities observed in vapor–gas-droplet wall jets can be analyzed using the local distributions of thermal and gas dynamic parameters across the boundary layer. The profiles of velocity (curve 1), steam concentration (2), gas temperature (3), liquid-phase temperature (4), and enthalpy (5) are shown in Fig. 5, where (a)—non-equilibrium conditions, (b)—equilibrium conditions, δ is the boundary-layer thickness. All the profiles are given in the relative form:

$$\frac{Q - Q_W}{Q_0 - Q_W} = f(y/R), \tag{22}$$

where Q, Q_W, and Q_0 are the values of parameters at the point of interest, on the wall, and in the flow core, respectively.

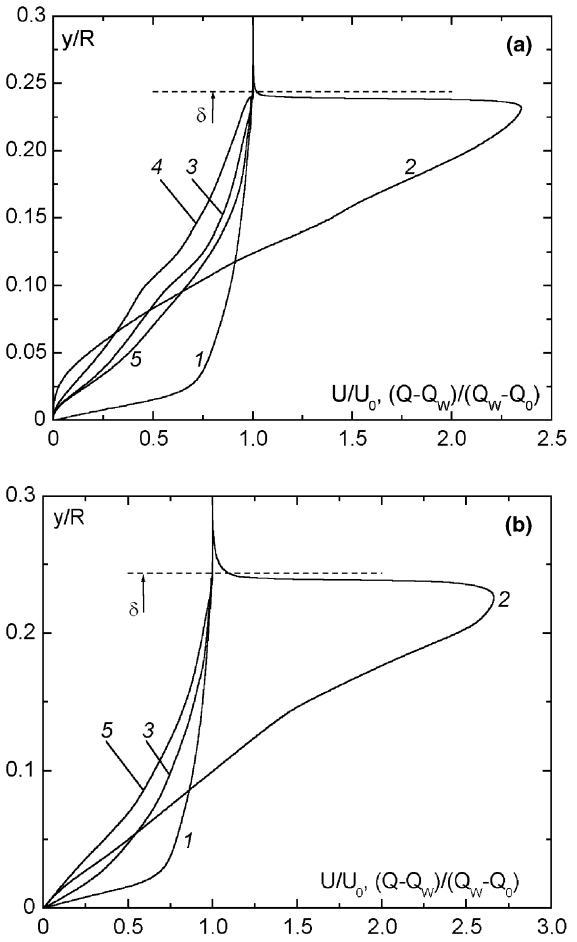

Fig. 5. The distributions of turbulent flow parameters on the pipe cross-section. Dotted line is the boundary layer thickness. $x/S = 50$; $m = 0.8$. (a) non-equilibrium regime with $T \neq T_L$; (b) equilibrium regime with $T = T_L$. The profiles of velocity U/U_0 (curve 1), steam concentration M_V (2), gas temperature T (3), liquid-phase temperature T_L (4), and enthalpy H (5).

As is seen from Fig. 5a, no similarity is observed between the distributions of physical quantities across the boundary layer. This is just what was expected because the energy and diffusion equations for the flow over an adiabatic wall lack the property of similarity. The phase transitions brought about by the evaporation processes make the absence of similarity even more pronounced; this mostly affects the vapor concentration distributions. The mass concentration profile of the vapor exhibits a distinct maximum, i.e., evaporation front [10]. Fig. 5b shows the distributions of parameters across the wall-screen boundary layer for the case of equilibrium evaporation regime; these distributions were calculated by the single-temperature, two-velocity model. No similarity in the distributions of parameters is observed here. The vapor-concentration maximum is somewhat higher than in the case of non-equilibrium evaporation regime, in which the temperatures of the phases are not identical. This behavior can be explained by the fact that all the heat supplied to the drop is spent for its evaporation.

The evaporation front position as a function of liquid-phase concentration is shown in Fig. 6, where $M_{V\max}$ is the coordinate of the steam concentration maximum. Normally, the evaporation front was observed near the upper boundary of the wall jet. The figure shows that, with increasing droplet concentration, the evaporation front moves closer to the flow core; on the contrary, with decreasing flow-core temperature it shifts to the wall. Thus, the data of Fig. 6 illustrate the general tendency in the behavior of screen characteristics as functions of initial thermal and gas dynamic conditions in the main and wall flows.

Fig. 7 illustrates variation of thermal efficiency Θ_T with the blowing parameter m at various concentrations of the liquid phase in the near-wall jet. As it could be expected, as the drop concentration increases, the parameter Θ_T also increases. The curves predicted for different concentrations behave similarly to the case of single-phase flow and are equidistant.

The predicted cooling efficiency of the two-phase gas-droplet screen is shown in Fig. 8. The shown values are dimensionless, representing the ratios between the efficiency of the two-phase screen, Θ_T, and the efficiency of the single-phase screen, Θ_{TA}, all thermal and gasdynamic conditions at the channel inlet except for the rate of coolant supply into the wall jet being identical. This representation clearly demonstrates the advantages of using a two-phase coolant instead of a single-phase coolant. The liquid phase present even in rather low mass concentrations (<5%) results in that the cooling efficiency increases by more than two-fold compared to

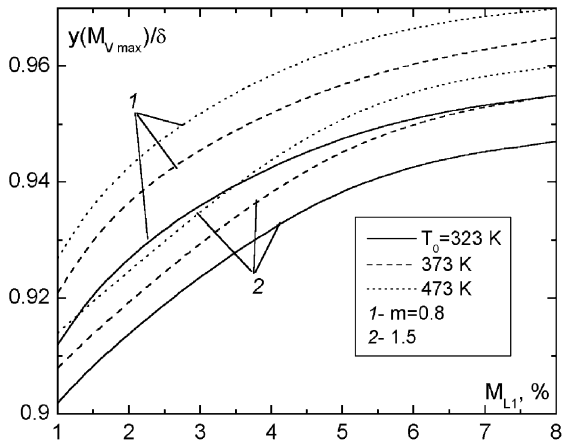

Fig. 6. The location of steam concentration maximum vs a change of liquid phase content in the near-wall jet. 1—$m = 0.8$; 2—1.5. $x/S = 50$.

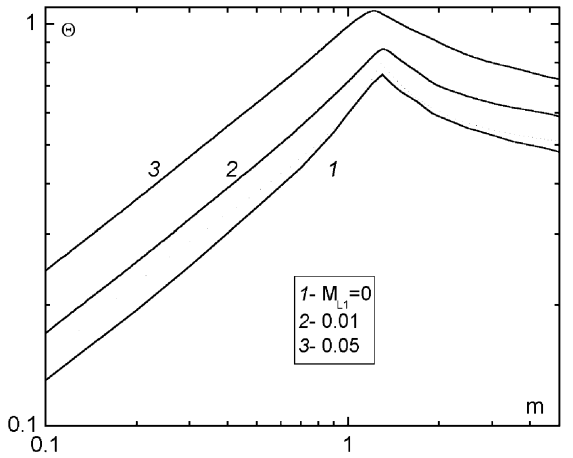

Fig. 7. Thermal efficiency of wall jets at various blowing parameter. $\frac{(x-x_0)}{Sm}Re_S^{0.25} = 5$; $T_0 = 373$ K $T_S = T_{L1} = 293$ K; $d = 30\,\mu$m. 1—$M_{L1} = 0$; 2—0.01; 3—0.05.

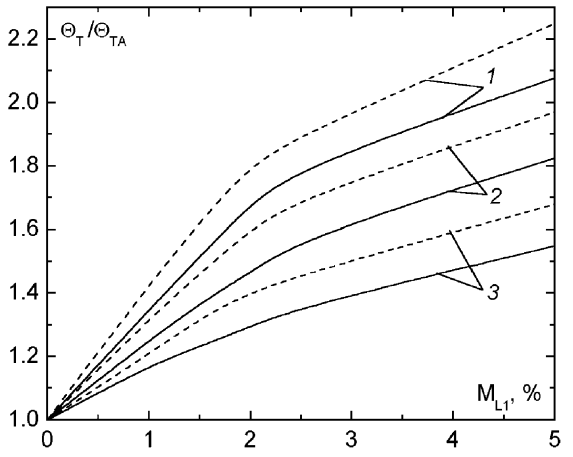

Fig. 8. The ratio between the effectiveness of two-phase jet and single-phase jet vs change concentration of dispersed phase. Lines $m = 0.8$; dotted lines $m = 1.5$. 1—$T_0/T_S = 1.1$; 2—1.27; 3—1.61; $x/S = 50$; $T_S = 293$ K.

the case of the single-phase flow. An increase in the main flow temperature substantially reduces the value of Θ_T. This can be explained by intensification of evaporation processes, prevailing at the external boundary of the jet-mixing layer, and not near the wall. Note yet another important regularity in Fig. 8. It is well known [1–4] that, as the injection parameter m decreases, the shielding properties of wall jets deteriorate because the rate of mass flow of the coolant decreases. With two-phase jets, these effects become even more pronounced since, according to Fig. 8, the Θ_T/Θ_{TA} ratio notably decreases with decreasing injection parameter.

An important question in the optimization of two-phase wall screens is the proper choice of liquid-drop sizes. Fig. 9 analyzes the effect of drop sizes on the distribution of thermal efficiency along the length of the channel. For particles smaller in size than several micrometers ($d_1 < 2$–5 μm) the thermal efficiency Θ_T/Θ_{TA} is independent of drop diameter, being determined exclusively by the mass content of the liquid drops in the flow. Of this range of sizes, equilibrium evaporation is typical, with the steam–gas mixture being in thermal equilibrium with the liquid phase. For larger particles ($d_1 > 5\,\mu$m), the thermal efficiency may be either decreasing (for large particles with $d_1 \approx 100\,\mu$m) or increasing function (for smaller particles with $d_1 = 30$–$50\,\mu$m). The increase in Θ_T/Θ_{TA} with increasing d_1 can be explained by the fact that, as the initial size of the disperse phase increases, the area of the contact surface between the steam–gas mixture and the liquid drops decreases markedly. More time is required for larger particles to be heated and evaporated. Thus, it can be noted that the optimum particle size in thermal protection of adiabatic walls under given conditions is 30–50 μm. Drops of such sizes are efficient in protecting walls at large distances from the exit plane of the slot used to inject the cooling jet flow into the channel.

It is known [1–6] that, in treating the screen efficiency in the case of foreign-gas blowing into the near-wall region or in the case of screens with phase transitions or chemical transformations, different definitions of the protection efficiency can adopted. For instance, the efficiency can be calculated from the temperatures, total enthalpies, or concentrations of the components. A comparison between the distributions of differently defined thermal efficiencies allows one to judge if similarity exists between heat- and mass-transfer processes in gas-drop screens with phase transitions.

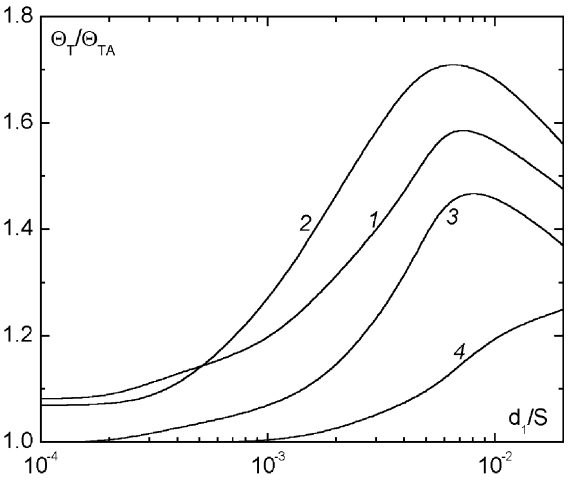

Fig. 9. The ratio between the effectiveness of two-phase near-wall screen Θ_T and gas jet Θ_{TA} vs change of initial dispersed phase diameter. $m = 0.8$; $M_{L1} = 0.05$. 1—$x/S = 25$; 2—50; 3—100; 4—200.

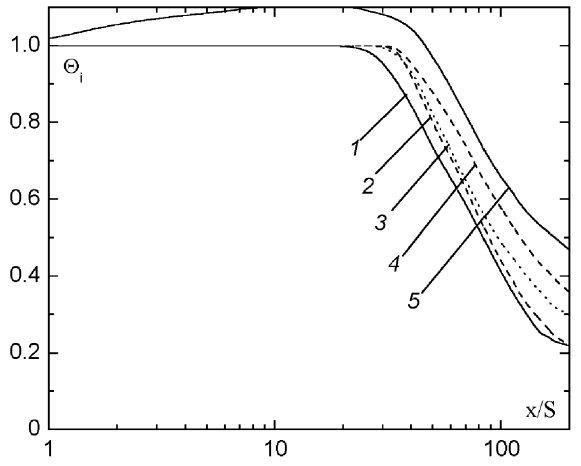

Fig. 10. Thermal efficiency of a wall gas-drop screen calculated from the gas temperature T (1), the enthalpy of the two-phase mixture (2), the drop concentration (3), the total concentration of liquid in the drops and water vapor (4), and the liquid-phase temperature T_L (5).

Fig. 10 illustrates the data calculated from the different thermal screen parameters. The profiles of the above-indicated parameters were calculated by the formula

$$\Theta_i = (\Psi_0 - \Psi_W)/(\Psi_0 - \Psi_S),$$

where Ψ is the parameter defined in terms of the gas temperature T (1), the enthalpy of the two-phase mixture (2), the drop concentration (3), the total mass of liquid in the drops and water vapor (4), and the liquid-phase temperature T_L (5). The enthalpy of the gas-drop mixture was calculated by the formula

$$H = \sum_{i=1}^{3} H_i M_i = H_A M_A + H_L M_L + H_V M_V,$$

where $H_i = \int C_{p,i} dT_i + h_i^0$ is the enthalpy of the i-th component with allowance for its formation energy (h_i^0) from simple substances. The highest value is displayed by the parameter Θ_L calculated from the droplet temperature. For this parameter, the thermal efficiency is in excess of unity, since the droplet deposited onto the wall undergo evaporation and assume a temperature lower than its equilibrium temperature at the exit plane of the slot. In the downstream region of initial flow region with $\Theta_T = 1$, all other efficiency parameters behave equidistantly, although the difference between them remains quite appreciable.

8. Conclusions

A calculation model is developed and a numerical heat and mass transfer study of a gas-droplet wall jet injected into the main airflow, performed. In studying complex mixing processes proceeding in two-phase wall jets, the Eulerian–Eulerian two-fluid model proved to yield rather adequate results. To close the transfer equations, the LRN k–$\tilde{\varepsilon}$ model of turbulence was used, extended to the case of flows with evaporating drops.

The addition of a small amount of droplets (not more than 5% of the total mass of the secondary gas flow) substantially (by a factor of 2) increases the screen efficiency. An increase in the main-flow temperature worsens the efficiency of the two-phase wall screen, intensifies the evaporation processes near the upper boundary of the jet flow, and leads to a more rapid boundary-layer heating.

The steam concentration profile displays a distinct maximum, i.e., evaporation front, normally observed near the upper boundary of the jet flow, where evaporation processes proceed most vigorously.

Acknowledgement

This work was supported by the Russian Federation's Presidential Foundation for Leading Scientific Schools (Grant No. 1308.2003.8) and Russian Academy Program (project 3.5.2.). M.A. Pakhomov thanks Russian Science Support Foundation for their grant for Young Ph.D. Scientist-2004. The authors are grateful to Prof. I. Derevich (Moscow State University of Environmental Ecology, Moscow), to Prof. L. Zaichik (Institute of High Temperature of RAS, Moscow) for fruitful discussions.

References

[1] S.S. Kutateladze, A.I. Leont'ev, Heat and Mass Transfer in Turbulent Boundary Layer, Hemisphere, New York, 1989.
[2] R.J. Goldstein, Film CoolingAdvances in Heat Transfer-1971, 7, 1971, pp. 321–378.
[3] V.M. Repukhov, The Theory of Thermal Shielding of a Wall by Gas Injection, Naukova Dumka, Kiev, 1980 (in Russian).
[4] E.P. Volchkov, Gas Near-Wall Screens, Nauka, Novosibirsk, 1983 (in Russian).
[5] G.N. Abramovich, T.A. Girshovich, S.J. Krasheninnikov, A.N. Sekundov, I.P. Smirnov, The Theory of Turbulent Jets, Nauka, Moscow, 1984, 718 p., (in Russian).
[6] A.I. Leont'ev, Heat and mass transfer problems for film cooling, ASME J. Heat Transfer 121 (1999) 509–527.
[7] E. Talmor, N. Weber, Foreign-gas film cooling along nonconverging and converging walls at various free-stream turbulence levels, in: Proceedings of the IV International Heat Transfer Conference, Paris, France, 1970, FC-8.7, 1–11.
[8] A.A. Vasil'ev, S.I. Kostjukov, V.M. Repukhov, A numerical calculation of gas-steam and liquid thermal screen over adiabatic wall with using enthalpy-moisture content dia-

gram, Promyshlennaya Teplotekhnika 5 (1983) 17–21 (in Russian).
[9] V.M. Repukhov, An effectiveness non-equilibrium gas-steam and liquid thermal screens, Promyshlennaya Teplotekhnika 8 (1986) 11–19 (in Russian).
[10] A.A. Vasil'ev, An effectiveness of gas-steam and liquid thermal screen behind a tangential slot, Promyshlennaya Teplotekhnika 10 (1988) 36–38 (in Russian).
[11] V.M. Repukhov, A.I. Neduzhko, The effectiveness of multicomponent non-equilibrium gas-steam and liquid thermal screens, in: Proceedings of Akad. of Sciences of Ukrainian SSR, Ser. A (1991) 83–87 (in Russian).
[12] V.I. Terekhov, K.A. Sharov, N.E. Shishkin, An experimental study of gas-stream mixing with a near-wall gas-drop jet, Thermophys. Aeromech. 6 (1999) 331–339.
[13] V.I. Terekhov, M.A. Pakhomov, K.A. Sharov, N.E. Shishkin, Simulation and experimental study of heat screen efficiency with injection of a gas-droplet jet, in: Proceedings of 4th International Conference on Multiphase Flow ISMF-2001, New Orleans, CD-ROM disc, Paper No. 702, 11 p., 2001.
[14] V.I. Terekhov, M.A. Pakhomov, Numerical investigation of the thermal efficiency of a two-phase gas-droplet wall screen in a cylindrical channel, High Temp. 40 (4) (2002) 586–593.
[15] V.I. Terekhov, K.A. Sharov, N.E. Shishkin, Heat shielding characteristics of two-phase gas-droplets screens in vertical cylindrical channel, Trans. of the Russian Academy of Sciences, Series Power Engineering (5) (2003) 111–119 (in Russian).
[16] V.I. Terekhov, M.A. Pakhomov, The modeling of a tube flow with injection of near-wall non-isothermal turbulent gas-droplets jet, in: Proceedings of the 5th International Conference on Multiphase Flow ISMF-2004, Yokohama, Japan, 2004. CD-ROM disc. Paper No. 135. 13 p.
[17] E.P. Volchkov, V.V. Terekhov, V.I. Terekhov, Flow structure and heat and mass transfer in boundary layers with injection of chemically reacting substances (review), Combust. Explo. Shock Wave. 40 (1) (2004) 1–16.
[18] V.I. Terekhov, M.A. Pakhomov, The numerical modeling of the tube turbulent gas-drop flow with phase changes, Int. J. Therm. Sci. 43 (6) (2004) 595–610.
[19] E.P. Volkov, L.I. Zaichik, V.A. Pershukov, Numerical Modeling of Combustion of Solid Fuel, Nauka, Moscow, 1994 (in Russian).
[20] M. Ishii, Thermo-Fluid Theory of Two-Phase Flows, Eyrolles, Paris, 1975.
[21] D.A. Drew, Mathematical modeling of two-phase flow, Ann. Revue Fluid Mech. 15 (1983) 261–291.
[22] A.A. Shraiber, L.B. Gavin, V.A. Naumov, V.P. Yatsenko, Turbulent Flows in Gas Suspensions, Hemisphere, New York, 1990.
[23] R.I. Nigmatulin, Dynamics of Multiphase Media, Hemisphere, Washington, 1991.
[24] C.T. Crowe, M. Sommerfeld, Y. Tsuji, Multiphase Flow with Droplets and Particles, CRC Boca Raton, Florida, USA., 1998.
[25] I.V. Derevich, The hydrodynamics and heat transfer and mass transfer of particles under conditions of turbulent flow of gas suspension in a pipe and in an axisymmetric jet, High Temp. 40 (1) (2002) 78–91.
[26] C.B. Hwang, C.A. Lin, Improved low-Reynolds-number k–$\widetilde{\varepsilon}$ model based on direct simulation data, AIAA J. 36 (1) (1998) 38–43.
[27] W.P. Jones, B.E. Lounder, The calculation of low-Reynolds-number phenomena with a two-equation model of turbulence, Int. J. Heat Mass Transfer 16 (6) (1973) 1119–1130.
[28] A.A. Mostafa, H.C. Mongia, On the modeling of turbulent evaporating sprays: Eulerian versus Lagrangian approach, Int. J. Heat Mass Transfer 30 (12) (1987) 2583–2593.
[29] K. Mastanaiah, E.N. Ganic, Heat transfer in two-component dispersed flow, ASME J. Heat Transfer 103 (2) (1981) 300–306.
[30] O. Simonin, Q. Wang, K.D. Squires, Comparison between two-fluid model predictions and large eddy simulation results in a vertical gas–solid turbulent channel flow, ASME Fluids Eng. Division Summer Meeting. FEDSM' 97-3625, 1997, 1–10.
[31] K.-C. Chang, M.-J. Shyu, Revisiting the Reynolds-averaged energy equation in near-wall turbulence model, Int. J. Heat Mass Transfer 43 (5) (2000) 665–676.
[32] J.D. Anderson Jr., G. Degrez, E. Dick, R. Grundmann, in: J.F. Wendt (Ed.), Introduction to Computational Fluid Dynamics, Springer-Verlag, Berlin, 1992, p. 291.
[33] D.A. Anderson, J.C. Tannehill, R.H. Pletcher, Computational Fluid Mechanics and Heat Transfer, Hemisphere, New York, 1984.